JOURNAL OF THEORETICAL
AND APPLIED MECHANICS
3, **36**, 1998

UNI-AXIAL LIQUEFACTION WAVE IN SATURATED SANDS

ANDRZEJ SAWICKI

Institute of Hydro-Engineering (IBW PAN), Gdańsk
e-mail: as@hapcio.ibwpan.gda.pl

A compaction theory is applied to description of stress wave propagation through saturated sands, including such associated phenomena as pore pressure generation and liquefaction. Numerical examples show that liquefaction is possible during either loading or unloading, depending on the magnitude of applied stress and mechanical properties of saturated sand. It is shown that the stress wave propagates without change of shapes but produces regrouping of the intrinsic stresses in matrix and fluid, i.e. generating excess pore pressure and reducing mean effective pressure, which leads to liquefaction. Those effects are caused by permanent porosity changes due to rearrangement of the granular structure of the sand, and pore water compressibility.

Key words: liquefaction, pore pressure, saturated soils, waves

1. Introduction

Mechanics of fluid-saturated granular materials has attracted attention in various branches of science and engineering being of particular importance in geophysics and civil engineering. Geophysicists are mostly interested in the propagation of stress waves through geologic media, including saturated soils and porous rocks, in order to investigate the structure of the Earth or to discover oil deposits. Prediction of the dynamic behaviour of saturated soils is of importance in many engineering problems including those related to earthquakes and soil-structure interactions. Relatively little attention has been paid to the mechanics of fluid-saturated granular materials by marine engineers investigating the behaviour of seabeds under various loading conditions, including water waves action and underwater explosions.

A major interest in marine engineering is to investigate the influence of the seabed on the propagation of water waves. The most simple approach is

based on the assumption that a seabed can be modelled as a porous and rigid (non-deformable) material. The flow of pore water is assumed to obey some empirical law (usually Darcy's law), which relates the fluid velocity to the pore pressure gradient by the coefficient of permeability. Such an approach is called filtration theory. The filtration theory has been applied to analysis of the influence of a permeable seabed on water waves propagation and sediment motion, see Hunt (1959), Liu (1973), Martin (1970), Massel (1976), Putnam (1949), Reid and Kajiura (1957). The permeable seabed and boundary conditions at the water-seabed interface allow for a more realistic formulation of the hydrodynamical problem. However, the pore pressures determined in the above approaches are independent of the seabed porosity and permeability.

Moshagen and Tørum (1975) take into account the pore fluid compressibility, which leads to a diffusion equation for pore pressures, and displays the importance of fluid compressibility on pore pressure distribution in the upper layers of the seabed. Moshagen and Tørum retain the assumption of seabed rigidity, which is criticised by Prevost et al. (1975). As an alternative they propose a model of a deformable seabed with pore fluid trapped in the pores (undrained conditions). The behaviour of such a material can be analysed using standard elasticity solutions, which show that the pore pressure changes occur not only in the vicinity of a mudline but also at substantial depths in the seabed. These papers display how solution to the same problem of pore pressure changes in a seabed due to the action of water waves yields substantially different results when using the different approaches. It is not always possible to settle experimentally which theoretical model describes better the real seabed behaviour. Mallard and Dalrymple (1977) point out that laboratory and field investigations can lead to extremely different conclusions.

The approach of Madsen (1978) and Yamamoto et al. (1978) takes into account the deformability of both solid skeleton and pore fluid in the analysis of seabed behaviour due to water waves. They make use of the more general theory of Biot (1956), who was the first to propose a rational approach to the mechanics of fluid-saturated porous solids. Foda (1989) shows an example of further developments, taking into account viscous properties of the boundary layer at the bed-water interface in the damping of water waves propagating over a soft bed.

The above papers dealing with the propagation of water waves over a seabed display difficulties in establishing proper boundary conditions at the water-seabed interface for the hydrodynamic problem. The main question of how the seabed behaves under real loading conditions is far from understood. The most general approach discussed is based on Biot's theory assuming a

compressible fluid and elastic skeleton. Those assumptions limit possible applications, particularly under extreme loading conditions, such as those during severe storms, earthquakes or underwater explosions. In these cases phenomena such as permanent pore pressure generation and soil liquefaction occur.

Soil liquefaction is designated as the process of transforming an initially solid material into a fluid in regard to the flow behaviour. Liquefaction is preceded by progressive pore pressure build-up. The increasing pore pressure changes the distribution of total pressure between the constituents of the saturated material reducing the so-called effective stresses. This means that the contact forces between grains decrease, so the material, on the macroscopic scale, becomes weaker. In the extreme case of liquefaction, these contact forces vanish and the material behaves macroscopically as a liquid.

The importance of liquefaction has been recognised by geotechnical engineers. Extensive reviews of the subject are provided by Zienkiewicz et al. (1978), Finn (1982), Ishihara and Towhata (1982), Martin and Seed (1982). A common approach accepted in geotechnical engineering is that the dynamic loads, within the range of low frequencies, can be simulated by quasi-static cyclic loadings. This very simplified assumption has allowed for the analysis of many problems of practical importance. However, there is still a wide range of problems which cannot be analysed using such simple approaches. An important example is blast-induced liquefaction, cf Studer and Kok (1980), Charlie et al. (1980). Although major efforts have been devoted to this problem, little progress has been made in understanding the phenomenon, see Rawlings (1987). In the opinion of Fragaszy and Voss (1982), there was no generally accepted theory to explain the blast-induced liquefaction mechanism, or to predict the occurrence and effects of blast-induced liquefaction.

There are several civilian and military aspects related to blast-induced soil liquefaction. For example, explosive and surface impacting loads have been used to induce a liquefaction condition when subsequent resolidification increases the density of loose granular deposits and fills. Blast-induced liquefaction may cause dams, dykes, embankments or natural slopes to fail by inducing sufficient excess pore water pressures which reduce the soil strength and allow gravity to fail the slopes. Liquefaction may also produce flotation, sinking or differential movements of structures, Charlie et al. (1980). For safety precautions in the design of military constructions and for the protection of, for example, dikes and storm surge barriers, an understanding of liquefaction due to explosions is of considerable importance.

Blast-induced liquefaction is also of importance in geophysics and geology. Charlie et al. (1980) mention laboratory and field air blast loading tests on wet

sands, and tests performed in Canada in 1971, when a 500-ton explosive was detonated at a site which consisted of ancient glacial lake sediments composed of alternating layers of sands, silts and clays. Liquefaction induced submarine slides are among the major threats to the security of seafloor structures, man-made reservoirs and seafloor networks, and create also a very important mechanism for transporting sediment from the deltaic to the offshore prodelta environment. At present we know very little about the behaviour of the soil mass during its transport downslope. Numerical models presently employed to simulate such sediment transport, as the turbulent flow and the viscous debris flow models, differ widely in their predictions. Consequently, we cannot predict with any certainty the forces exerted by a submarine *sediment avalanche* on structures anchored onto the seafloor. The liquefaction front of marine sediments is a key element in understanding how a sediment failure develops, cf Syvitski and Schafer (1990).

The mechanics of soil liquefaction touches two, traditionally distinct disciplines; namely, the mechanics of solids and fluid mechanics. In soil mechanics it is usually sufficient to recognise that under certain loading conditions a saturated soil is going to liquefy. The question of what happens after liquefaction, when the material behaves as a fluid, has not been answered. On the other hand, fluid mechanics has already recognised a need for more realistic formulations of such problems as those noted in the earlier discussion of the propagation of water waves, but attempts have been limited to very simple models of the seabed leading conclusions not always satisfactory. There is, therefore, a need for a more general approach to the problems involving soil liquefaction.

In this paper a simple description of a uni-axial, blast-induced liquefaction of saturated sand is presented. A starting point for the analysis presented is the compaction theory of saturated granular materials proposed by Morland and Sawicki (1983), (1985). The compaction theory allows determining of pore pressure generation due to a permanent rearrangement of the soil's granular structure. The shear response of saturated sand is defined by a non-linear hypoelastic relation which takes into account the degradation of material properties during pore pressure generation. The model incorporates basic features of the behaviour of saturated sands subjected to dynamic loads. Sawicki and Morland (1985) applied the model to shear propagation through a saturated layer induced by a cyclic horizontal acceleration of its base. Numerical solutions obtained, prior to liquefaction, were in qualitative agreement with empirical data, but the model does not apply after liquefaction.

First, the compaction theory is outlined and the governing equations for

uni-axial displacement are derived. Then, an analysis of wave propagation is presented using the method of characteristics. The theoretical results are illustrated by numerical examples describing the response to surface loading in which the stress monotonically increases to a maximum value and then decreases back to zero. Such a pulse simulates a blast loading, see Charlie et al. (1980). The results are discussed for various soil parameters, and demonstrate that a simplified theory is valid. The results obtained also support some heuristical suggestions of Charlie et al. (1980) regarding the possible mechanism of blast-induced liquefaction, that is the permanent volume reduction during loading leads to the generation of excess pore pressure and liquefaction.

2. Compaction model

The compaction Φ is defined as an irreversible infinitesimal porosity change due to the rearrangement of granular structure

$$\frac{n_0 - n}{n_0} = \Delta + \Phi \tag{2.1}$$

where

n_0 – initial porosity
n – porosity
Δ – reversible, infinitesimal, porosity decrease.

The total volumetric change of the saturated sand follows from the porosity changes if an assumption of solid grain incompressibility is accepted, thus

$$\epsilon = n_0 - n = n_0\Delta + n_0\Phi = \epsilon^{el} + \epsilon^{\Phi} \tag{2.2}$$

where ϵ is measured positive in compression. The reversible (elastic) porosity changes are given by

$$\Delta = ap^s - bp^f \tag{2.3}$$

p_s and p_f denote partial pressures in the solid and fluid phases, respectively

$$a = \frac{1 - n_0}{n_0}\kappa \qquad b = \frac{1 - n_0}{n_0}[a - \kappa_f] \tag{2.4}$$

κ is the skeleton compressibility and κ_f is the pore fluid compressibility, see Morland (1978). It is more convenient, instead of using partial pressures, to

introduce the pore pressure u. Now $p^s = p - p^f$ and $p^f = n_0 u$, where p is the total mean pressure, so Eq (2.3) takes the form

$$\Delta = ap - \Big[a - (1 - n_0)\kappa_f\Big]u = ap - \beta u \tag{2.5}$$

Similar relations hold between pressure and dilatation increments

$$d\epsilon = d\epsilon^{el} + d\epsilon^{\Phi} \tag{2.6}$$

where

$$d\epsilon^{el} = n_0 a dp - n_0 \beta du \qquad d\epsilon^{\Phi} = n_0 d\Phi \tag{2.7}$$

The compaction is governed by the evolutionary law

$$\frac{d\Phi}{d\xi} = D_1 K \exp(-D_2 \Phi) \tag{2.8}$$

where

K – certain invariant of the strain tensor $\boldsymbol{\epsilon}$

D_1, D_2 – coefficients which have to be determined experimentally for a given sand

ξ – monotonic increasing loading parameter.

Morland and Sawicki (1983) defined K as the second invariant of deviatoric reversible strain

$$K = \frac{1}{2} \operatorname{tr} \hat{\boldsymbol{\epsilon}}^2 \qquad \hat{\boldsymbol{\epsilon}} = \boldsymbol{\epsilon}^{el} - \frac{1}{3} \operatorname{tr} \boldsymbol{\epsilon}^{el} \mathbf{I} \tag{2.9}$$

The loading parameter is defined as accumulated deviatoric elastic strain, the increment of which is always positive

$$d\xi = \sqrt{\Big|\frac{1}{2} \operatorname{tr} (d\hat{\boldsymbol{\epsilon}}^2)\Big|} \tag{2.10}$$

A reversible shear response of the sand is described by the hypoelastic deviatoric relation

$$\frac{d\hat{\boldsymbol{\sigma}}}{d\xi} = 2G(p') \frac{d\hat{\boldsymbol{\epsilon}}}{d\xi} \tag{2.11}$$

where $\hat{\boldsymbol{\sigma}} = \boldsymbol{\sigma} - \frac{1}{3}(\operatorname{tr} \boldsymbol{\sigma})\mathbf{I}$ is the stress deviator, and G is a generalised shear modulus. For small strains it is convenient to use the following form of the function G

$$G = G_0 + G_1 \sqrt{p'} \tag{2.12}$$

where G_0 and G_1 are coefficients which have to be determined experimentally for a given sand. p' is a mean effective pressure defined as

$$p' = p - u \tag{2.13}$$

The shape of the function G, expressed by Eq (2.12), is consistent with various experimental data, see Das (1983). The quantity G_0 denotes a residual shear modulus at zero effective pressure. Note that Eq (2.12) describes the degradation of shearing resistance of saturated sand during pore pressure generation.

3. Incremental relations for uni-axial deformation

Uni-axial deformation of sand is of great importance. First, one-dimensional models of sand behaviour are still very useful in geotechnical practice, since they can serve as a good approximation of the real ground behaviour and allow for simple solutions of basic problems. As an example the one-dimensional consolidation model of Terzaghi is still applied to estimate soil settlement. Secondly, one-dimensional consolidometers are available in a standard geotechnical laboratory to test theory and predictions.

Let us consider a uni-axial deformation of saturated sand in the z direction. The lateral deformation is zero. The sand is subjected to an initial stress state described by a longitudinal stress σ_z^0 and a lateral stress σ_x^0, measured positive in compression. The initial value of pore pressure is assumed to be zero, so the initial effective stresses are respectively $\sigma_z'^0 = \sigma_z^0$ and $\sigma_x'^0 = \sigma_x^0$. Drainage of pore water is prevented (undrained conditions). The case when the vertical stress increases from its initial value σ_z^0 to its maximum value $\sigma_z^{\max}$, and then decreases back to σ_z^0, is considered. During the loading both reversible and irreversible porosity changes are allowed, which is different from the commonly adopted assumption that under undrained conditions the total porosity change can be neglected as a first approximation, see Morland and Sawicki (1983). The total volumetric change is therefore the result of the pore fluid compression. In turn, the intrinsic volume change of the pore water is related to the porosity change by

$$\epsilon^f = \frac{n_0 - n}{n_0} = \frac{\epsilon}{n_0} \tag{3.1}$$

Also

$$\epsilon^f = \kappa_f u \tag{3.2}$$

so that

$$\epsilon = n_0 \kappa_f u \qquad \text{or} \qquad d\epsilon = n_0 \kappa_f du \tag{3.3}$$

From Eqs (2.2) and (3.2) it follows that

$$u = \frac{1}{a + n_0 \kappa_f}(ap + \Phi) \tag{3.4}$$

The two equations describing the shear and compaction (Eqs (2.8) and (2.11)) are

$$d\epsilon_z^{el} = \frac{1}{2G}(d\sigma_z - d\sigma_x) \tag{3.5}$$

and

$$d\Phi = \frac{D_1}{3\sqrt{3}}\left(\epsilon_z^{el}\right)^2 \exp(-D_2\Phi) d\epsilon_z^{el} = C d\epsilon_z^{el} \tag{3.6}$$

where ϵ_z^{el} denotes the z component of the elastic strain tensor $\boldsymbol{\epsilon}^{el}$. The total volumetric deformation is equal to the vertical deformation, so $d\epsilon = d\epsilon_z$ and $d\epsilon^{el} = d\epsilon_z^{el}$, $d\epsilon^{\Phi} = d\epsilon_z^{\Phi}$. Eqs (2.6) and (2.7) then become

$$d\epsilon_z = n_0 a dp - n_0 \beta du + n_0 d\Phi = d\epsilon_z^{el} + d\epsilon_z^{\Phi} \tag{3.7}$$

using

$$dp = \frac{1}{3}(d\sigma_z + 2d\sigma_x) \tag{3.8}$$

Eq (3.3) becomes

$$d\epsilon_z = n_0 \kappa_f du \tag{3.9}$$

The four equations (3.5)÷(3.7) and (3.9) describe the deformation of saturated sand under a given vertical stress σ_z, in one-dimensional compaction in the case of loading ($d\sigma_z > 0$). The various associated relations are

$$\begin{aligned} d\epsilon_z^{el} &= \frac{B_1}{1 + B_2 C} d\sigma_z = B d\sigma_z & d\Phi &= CB d\sigma_z \\ d\sigma_x &= (A_1 + A_2 CB) d\sigma_z & d\epsilon_z &= B(1 + n_0 C) d\sigma_z \\ du &= \frac{B(1 + n_0 C)}{n_0 \kappa_f} d\sigma_z \end{aligned} \tag{3.10}$$

where

$$A_1 = \frac{1-\alpha+\frac{\beta}{\kappa_f}}{1+2\alpha+\frac{\beta}{\kappa_f}} \qquad A_2 = \frac{2Gn_0\left(\frac{\beta}{\kappa_f}\right)}{1+2\alpha+\frac{\beta}{\kappa_f}}$$

$$B_1 = \frac{3\alpha}{2G\left(1+2\alpha+\frac{\beta}{\kappa_f}\right)} \qquad B_2 = \frac{n_0\left(\frac{\beta}{\kappa_f}\right)}{1+2\alpha+\frac{\beta}{\kappa_f}} \tag{3.11}$$

$$\alpha = \frac{2}{3}Gn_0 a$$

The function C is defined in Eq (3.6). The system of equations (3.10) is non-linear, so for a given longitudinal stress history, up to the point corresponding to liquefaction, a solution must be determined numerically.

The simple liquefaction condition commonly adopted is that the effective pressure is zero, Morland and Sawicki (1983)

$$\text{liquefaction}: \quad p' = 0 \tag{3.12}$$

after which the macroscopic response of saturated sand dramatically changes. The shearing resistance of the solid grains-pore fluid mixture is very small, since $G = G_0 \cong 0$, so this mixture can be treated macroscopically as a fluid. There is no established constitutive law for such a mixture (the concentration of suspended grains is greater than 60%). Some authors, cf e.g. Foda (1989), proposed a viscoelastic model for a boundary layer at the bed-water interface, which perhaps might be appropriate for cohesive suspensions (clayey soils), but not necessarily for liquefied sands. An elementary post-liquefaction law would be to assure that the mixture behaves like an elastic fluid, the compressibility of which is given by

$$\kappa_m = n_0\kappa_f \tag{3.13}$$

Eq (3.13) follows from a simple estimation of the mixture compressibility: $\kappa_m = n_0\kappa_f + (1-n_0)\kappa_s$, where κ_s is the compressibility of solid grains. Usually $\kappa_s \approx \kappa_f/30$, so Eq (3.13) is a good approximation, cf Lambe and Whitman (1969). This ignores the viscous shear response however.

Unloading $(d\sigma_z < 0)$ is governed by Eqs (3.10) with the additional assumption that no compaction takes place $(C = 0)$. The respective increments are given by the following equations

$$d\sigma_x = A_1 d\sigma_z \qquad d\epsilon_z^{el} = B_1 d\sigma_z \qquad du = \frac{B_1}{n_0\kappa_f}d\sigma_z \tag{3.14}$$

where the functions A_1 and B_1 are defined by Eqs $(3.11)_{1,3}$.

4. Equations of motion

The case of undrained conditions is considered, so there is no relative motion of the solid skeleton and pore fluid and there is a single common velocity field

$$\boldsymbol{v}^s = \boldsymbol{v}^f = \boldsymbol{v} \tag{4.1}$$

where $\boldsymbol{v}^\alpha$ denotes the particle velocity of the respective constituent ($\alpha = s$ for solid skeleton, $\alpha = f$ for pore fluid), and $\boldsymbol{v}$ is the common velocity. Assumption (4.1) means that the drag force between the constituents prevents relative motion. In the case of rapid loading, such as during explosions, there is little time for relative motion, so the undrained assumption is realistic and pore pressure is not dissipated. When compressional waves propagate through fluid-saturated elastic porous media with the assumption (4.1) accepted, the two wave fronts coalesce into a single front, Garg et al. (1973).

The linear momentum balance equations for the two constituents, in the uni-axial case, are

$$-\frac{\partial \sigma_z^s}{\partial z} = \rho_0^s \frac{\partial v}{\partial t} \qquad -\frac{\partial \rho^f}{\partial z} = \rho_0^f \frac{\partial v}{\partial t} \tag{4.2}$$

where $\rho_0^\alpha (\alpha = s, f)$ denotes the partial density of the respective constituent, σ_z^s is the partial stress in the solid phase, Morland and Sawicki (1983). Addition of Eqs (4.2) gives the equation of motion for the mixture:

$$-\frac{\partial \sigma_z}{\partial z} = \rho \frac{\partial v}{\partial t} \tag{4.3}$$

since

$$\sigma_z = \sigma_z^s + p^f \tag{4.4}$$

and

$$\rho = \rho_0^s + \rho_0^f \tag{4.5}$$

The compressive strain ϵ_z is related to the longitudinal displacement U by

$$\epsilon_z = -\frac{\partial U}{\partial z} \tag{4.6}$$

hence

$$\frac{\partial \epsilon_z}{\partial t} = -\frac{\partial v}{\partial z} \tag{4.7}$$

It is convenient to present Eqs (4.3) and (4.7) in non-dimensional form by introducing typical units; namely, stress unit $S_0 = 10^5\,\mathrm{N/m^2}$, strain unit

$E_0 = 10^{-3}$, modulus unit $10^8\,\mathrm{N/m^2}$, and compressibility unit $10^{-8}\,\mathrm{m^2/N}$. Let H denote a characteristic distance and t_0 a characteristic time. The non-dimensional longitudinal co-ordinate is then $Z = z/H$, the non-dimensional time is $T = t/t_0$, the non-dimensional stress is $\sigma = \sigma_z/S_0$, and the non-dimensional strain is $\epsilon = \epsilon_z/E_0$. It is also convenient to introduce a separate particle velocity unit V_0, so the non-dimensional particle velocity is $V = vH/V_0$ and t_0 will be chosen to define the ratio of characteristic distance and time, H/t_0, as the magnitude of the wave velocity, which in general is much larger than the particle velocity. Eqs (4.3) and (4.7) take the following non-dimensional form

$$\frac{\partial \sigma}{\partial Z} + \alpha_1 \frac{\partial V}{\partial T} = 0 \qquad \frac{\partial V}{\partial Z} + \beta_1 \frac{\partial \epsilon}{\partial T} = 0 \tag{4.8}$$

where

$$\alpha_1 = \frac{\rho V_0 H}{S_0 t_0} \qquad \beta_1 = \frac{E_0 H}{t_0 V_0} \tag{4.9}$$

Eliminating the non-dimensional strain ϵ from Eq $(4.8)_2$ gives

$$\frac{\partial \sigma}{\partial Z} + \alpha_1 \frac{\partial V}{\partial T} = 0 \qquad \frac{\partial V}{\partial Z} + \alpha_2 \frac{\partial \sigma}{\partial T} = 0 \tag{4.10}$$

where α_1 is defined in Eq (4.9)

$$\alpha_2 = B\beta_1(1 + n_0 C) \tag{4.11}$$

B and β_1 are defined by Eqs $(3.10)_1$ and (4.9), and C is defined in Eq (3.6). Eqs (3.10) are already expressed in non-dimensional form.

The system of equations (4.10) is hyperbolic, with characteristics given by

$$\frac{dZ}{dT} = \pm\zeta \qquad \zeta = \sqrt{\frac{1}{\alpha_1 \alpha_2}} \tag{4.12}$$

The following relations hold along the characteristics

$$\begin{aligned} d\sigma + \eta dV = 0 \qquad \text{along} \qquad \frac{dZ}{dT} = \zeta \\ d\sigma - \eta dV = 0 \qquad \text{along} \qquad \frac{dZ}{dT} = -\zeta \end{aligned} \tag{4.13}$$

where

$$\eta = \sqrt{\frac{\alpha_1}{\alpha_2}} \tag{4.14}$$

Following Morland (1959) it can be shown that the values of σ and V are constant along the respective positive characteristics, hence the characteristics (4.12) are straight lines, for a pulse propagating into a uniform region throughout which there is a common stress-strain $(\sigma - \epsilon)$ relation.

5. Numerical examples and discussion

The following physical parameters have been adopted: initial porosity $n_0 = 0.375$, density of sand grains (quartz) $\rho_s = 2600\,\mathrm{Ns^2/m^4}$, density of pore water $\rho_w = 1000\,\mathrm{Ns^2/m^4}$, $H = 100\,\mathrm{m}$, $t_0 = 0.2724\,\mathrm{s}$, $V_0 = 0.1676\,\mathrm{m/s}$. The density of the mixture, from Eq (4.5), is

$$\rho = n_0\rho_w + (1 - n_0)\rho_s = 2000\ \mathrm{Ns^2/m^4} \tag{5.1}$$

The following initial stress state is assumed: $\sigma_z^0 = 0.5$ and $\sigma_x^0 = 0.3$.

The first example illustrates the influence of soil parameters such as coefficients describing compaction D_1 and D_2, shear modulus G_1 (residual shear modulus $G_0 = 0$), skeleton compressibility a, and pore fluid compressibility κ_f, on the onset of liquefaction.

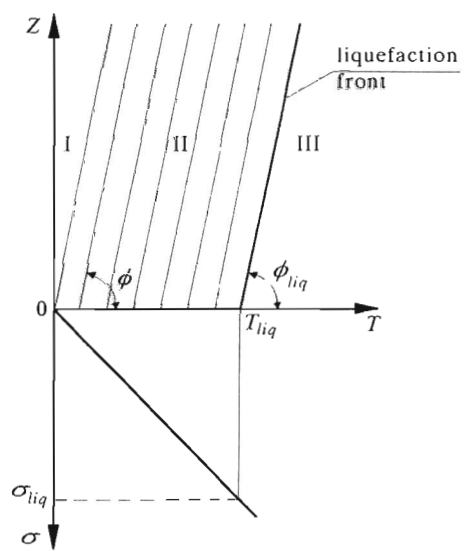

Fig. 1. Loading prior to liquefaction – positive characteristics. Medium dense sand: $D_1 = 5$, $D_2 = 0.2$, $G_1 = 1$, $a = 1.75$, $\kappa_f = 0.05$

Fig.1 presents positive characteristics in the T, Z plane during loading prior to liquefaction, for a medium dense saturated sand. The stress at $Z = 0$ increases linearly with time, so the initial pulse (during loading) is given by

$$\sigma(Z = 0) = p_1 T \tag{5.2}$$

where the coefficient p_1 describes the rate of stress increase. According to Valliapan and Ang (1988) a precise description of the pressure-time history

for blast loading in sand is difficult to obtain. The duration of an explosion is less than 20 milliseconds, Cole (1965). The maximum pore pressure caused by an explosion in sand does not exceed $10^8\,\mathrm{N/m^2}$ ($\sigma_{\max} = 10^3$ in our units) according to Ricker (1977). Nowacki and Raniecki (1987) suggest that the maximum peak stress during explosions is in the range of $10^7 \div 10^9\,\mathrm{N/m^2}$. For example, $p_1 = 5 \times 10^4$ corresponds to the peak stress $\sigma_{\max} = 10^3$ ($10^8\,\mathrm{N/m^2}$) which develops in a rise time of 2×10^{-2} s. The characteristics presented in Fig.1 were computed numerically from Eqs *(3.10)*, *(3.11)* and *(4.12)*.

The positive characteristics shown in Fig.1 are almost parallel to each other. The slope of the initial characteristic is 4.5054 which corresponds to the angle $\phi = 77.485°$. During loading the angle ϕ slightly increases, reaching its maximum value of $77.4957°$ for $\sigma = 15.9$. Further loading causes a decrease of ϕ, again very slowly. Just prior to liquefaction $\phi_{liq} = 77.3017°$. Stress increments travel with speeds defined by the slopes of associated characteristics, with the initial stress increment speed defined by the slope of the first characteristic. The physical velocity of stress propagation is

$$c = \zeta \frac{H}{t_0} = 367.107\zeta \tag{5.3}$$

so the initial speed is $c = 1654\,\mathrm{m/s}$. The maximum velocity corresponding to $\sigma = 15.9$ is $c = 1655\,\mathrm{m/s}$, and the velocity prior to liquefaction is $1629\,\mathrm{m/s}$. In practice this means that the stress pulse propagates essentially with a uniform speed and without any change of shape. During pore pressure generation (in region II) the velocity of propagation decreases only slightly, the difference being approximately 1.5%. Paterson (1956) reports that the velocity of wave propagation in water-filled sands is in the range $1650 \div 1690$ (± 30) m/s.

The velocity of compressive wave propagation in saturated sand can be estimated by Eq (4.12). Assuming that $1 + n_0 C \cong 1$ and $a + n_0\kappa_f \cong a$, then

$$\zeta \cong \frac{1}{\sqrt{\alpha_1 \beta_1 n_0 \kappa_f}} \tag{5.4}$$

A typical water compressibility is $\kappa_f = 0.05$ ($\times 10^{-8}\,\mathrm{m^2/N}$), so for the assumed data $\zeta = 4.4483$, which corresponds to a real velocity of $1633\,\mathrm{m/s}$. This brief analysis shows that the water compressibility governs the speed of stress wave propagation through the saturated sand. The influence of other soil parameters is much smaller, and can be neglected in the first approximation.

The influence of various soil parameters on the onset of liquefaction is presented in Table 1. The above conclusion that water compressibility is the main factor governing the speed of wave propagation is fully supported by the

numerical analysis of the full system of equations. Further inspection reveals that there are two main parameters which influence the value of the stress σ_{liq} corresponding to the onset of liquefaction, namely the water compressibility κ_f and the compaction coefficient D_1. The influence of other parameters like D_2, G and a is much smaller. As already mentioned, a typical water compressibility is $\kappa_f = 0.05$. The value 0.1 may be appropriate to a mixture of water and air. Adopting $\kappa_f = 0.05 = \text{const}$, there remains one significant parameter governing the stress level corresponding to liquefaction, namely D_1. The coefficient D_1 is small for dense sands ($D_1 < 3$) and increases with the susceptibility of sand to compaction. Values $D_1 > 10$ correspond to loose sands.

Table 1. Influence of saturated sand parameters on the onset of liquefaction

n_0	D_1	D_2	G_1	a	κ_f	$\phi_{initial}$ [°]	σ_{liq}	ϕ_{liq} [°]
1	5	0.2	1	1.75	0.05	77.486	323.4	77.302
2	20	0.2	1	1.75	0.05	77.486	158.1	77.283
3	20	0.2	1	1.75	0.1	72.776	79.6	72.239
4	5	0.2	1	1.75	0.1	72.776	163.3	72.288
5	5	0.2	1	1	0.1	72.899	147.2	72.229
6	5	0.2	0.5	1.75	0.05	77.441	321.6	77.302
7	20	0.1	1	1.75	0.05	77.486	146.2	77.276
8	20	0.3	1	1.75	0.05	77.486	174.7	77.294
9	40	0.2	1	1.75	0.05	77.486	119.0	77.277
10	10	0.2	1	1.75	0.05	77.486	218.8	77.292
11	8	0.2	1	1.75	0.05	77.486	245.9	77.295
12	3	0.2	1	1.75	0.05	77.486	475.2	77.313
13	5	0.2	1	0.5	0.05	77.641	270.0	77.227
14	5	0.2	1	0.2	0.05	77.949	258.8	77.070

Fig.2 illustrates the history of pore pressure u and the mean effective pressure p', prior to liquefaction, for the data from Fig.1. The pore pressure increases nearly linearly from its initial zero value. The mean effective pressure first increases from its initial value of 0.367 to its maximum value of 0.881 corresponding to $\sigma = 93$, and then decreases back to zero at the onset of liquefaction which corresponds to $\sigma_{liq} = 323.4$.

Note that along each positive characteristic, presented in Fig.1, the stress σ is constant, so from Fig.2 the pore pressure u and the effective pressure p' on each of the characteristics can be determined.

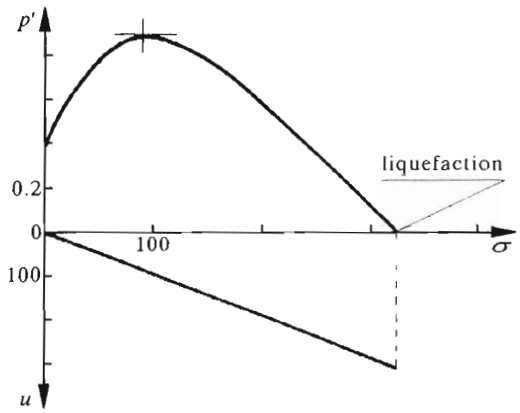

Fig. 2. History of pore pressure u and mean effective pressure p' prior to liquefaction. Data from Fig.1

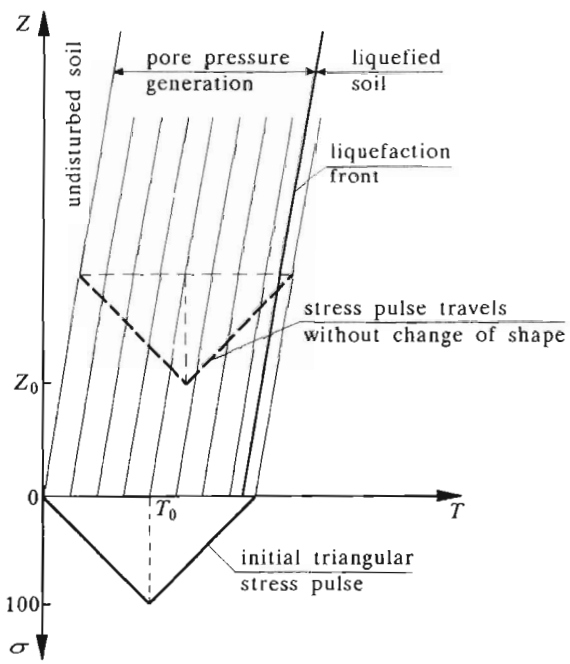

Fig. 3. Characteristic diagram for triangular loading-unloading stress pulses. Data from Fig.1. See also curves 1 in Fig.4

The results presented in Fig.2 can be compared with the results computed for a purely elastic mixture (no compaction; $C = 0$). For the same loading the character of the pore pressure changes is similar but with values a little smaller. For example, the stress $\sigma = 200$ produces a pore pressure $u = 192.4$ in the case of an elastic mixture against $u = 197.1$ in the case of compacting sand. The main difference is displayed by values of the effective pressure p'. In the case of an elastic mixture the effective pressure steadily increases from its initial value of 0.367 to 3.68 for $\sigma = 323$, whilst in the compacting material $p' = 0$ for $\sigma = 323.4$. For $\sigma = 200$, $p' = 2.43$ and 0.584, respectively. This is caused by the irreversible porosity changes in the saturated sand which produce additional (excess) pore pressure changes leading to the decrease of an effective pressure and subsequent liquefaction. Such effects cannot be described within the framework of elastic mixtures theories such as the Biot theory.

Fig.3 presents a characteristic diagram for a triangular loading-unloading stress pulse, which approximates the stress history caused by a weak explosion, Charlie et al. (1980). The peak stress is $\sigma = 100$ ($10^7\,\mathrm{N/m^2}$), and the rise time is T_0. Material properties are those presented in Fig.1. Liquefaction of such a material during loading occurs at $\sigma = 323.4$. A stress pulse travels without change of shape, and each characteristic carries particular information about the saturated sand behaviour, i.e, the stress σ is constant along each characteristic. Respective changes of pore pressure are shown in Fig.4 (curves marked 1). During the loading, pore pressure increases from its initial zero value to its maximum value of 97.85 corresponding to $\sigma = 100$. The effective pressure also increases to 0.881 at $\sigma = 93$, then slowly starts to decrease back to 0.877 at $\sigma = 100$. Unloading is elastic, and no pore pressure is generated. During unloading the effective pressure linearly decreases to zero at $\sigma = 16$, which corresponds to liquefaction. This interesting phenomenon, namely liquefaction during unloading, was observed experimentally by Fragaszy and Voss (1982), but for different loading conditions since their experiments were performed in triaxial apparatus. Liquefaction is produced by the excess pore pressure (Fig.4b) generated during loading.

The broken line $1'$ corresponds to the behaviour of a purely elastic mixture (the same data as in the case 1 except that D_1 is zero – no compaction). In this case the effective pressure increases linearly to a value of 1.403, and during unloading decreases to its initial value following the loading path in reverse. Note that the unloading line in case 1 is parallel to the line $1'$.

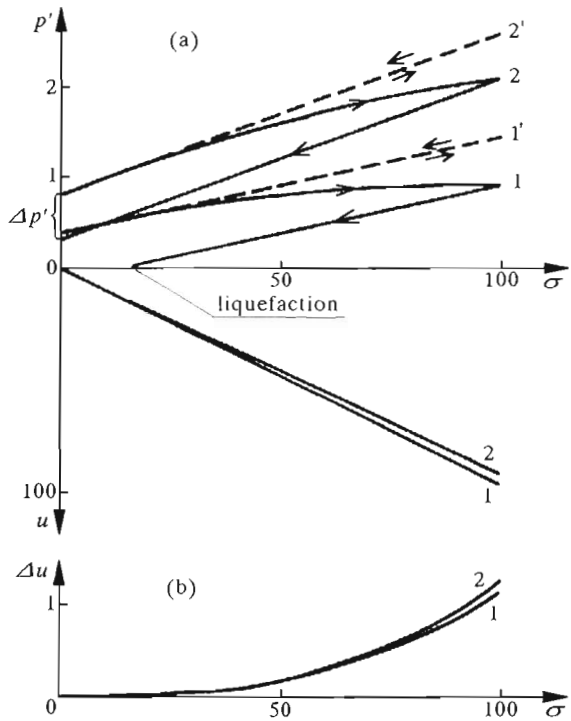

Fig. 4. (a) Pore pressure and effective pressure changes during loading and unloading; 1 – medium dense sand, 2 – dense sand. Broken lines illustrate the behaviour of purely elastic sand. (b) Excess pore pressures due to compaction

The diagrams marked 2 in Fig.4 correspond to a dense sand with small compaction susceptibility ($D_1 = 2$, $D_2 = 0.1$, $G = 2$, $a = 1$; $\kappa_f = 0.05$, $n_0 = 0.375$). Additionally, a larger initial stress state was assumed ($\sigma_z^0 = 1$, $\sigma_x^0 = 0.7$). A similar stress pulse does not produce liquefaction in this case, but it is seen that after unloading (the longitudinal stress σ returns to zero) the effective pressure is lower than its initial value shown by the decrease $\Delta p'$ in Fig.4a, which means that a residual excess pore pressure has remained in the saturated sand. This example supports field observations that dense sands are much less susceptible to blast-induced liquefaction than medium dense and loose ones, Rawlings (1987).

An alternative interpretation of the results presented in Fig.3 and Fig.4 is shown in Fig.5. The effective pressure p' and pore pressure u pulses are carried along positive characteristics, without any change of form. Note that at the onset of liquefaction the pore pressure $u = 16$.

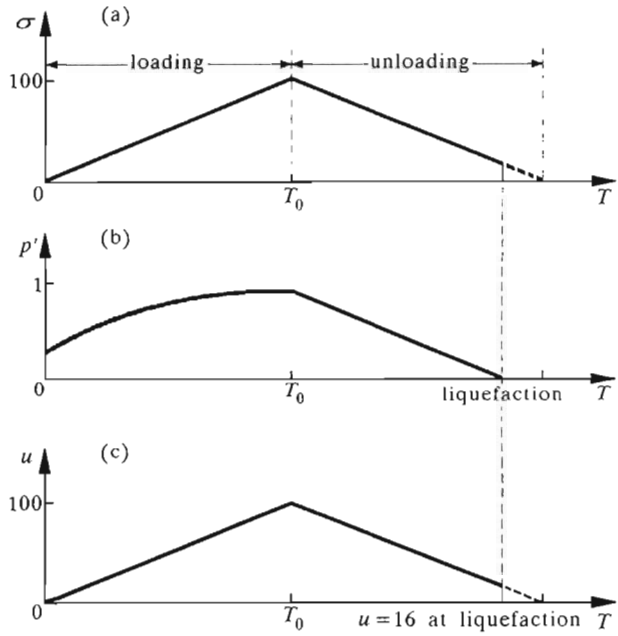

Fig. 5. Alternative interpretation of the results presented in Fig.3 and Fig.4

6. Conclusions

It has been shown that compaction theory can be applied to description of stress wave propagation through saturated sands, including such phenomena as associated pore pressure generation and liquefaction. One of the main conclusions which follow from a detailed analysis of the uni-axial wave propagation problem is that the shape of the stress wave propagates without change. This conclusion simplifies the analysis essentially.

The compaction theory differs essentially from the theories of saturated granular materials based on the Biot type approach, since it includes a description of permanent volume changes due to the re-arrangement of the granular structure.

Numerical examples show that liquefaction is possible during either loading or unloading, depending on the magnitude of applied stress and on the mechanical properties of the saturated sand. The liquefaction susceptibility of saturated sand depends mainly on two parameters; namely, the pore water compressibility κ_f and the coefficient D_1 appearing in the compaction law. Numerical results support an observation that it is easier to liquefy loose

sands than the dense ones. The results obtained also support some heuristic suggestions of Charlie et al. (1980) regarding the possible mechanism of blast-induced liquefaction, that is, the permanent volume reduction during loading leads to the generation of excess pore pressure and subsequent liquefaction.

Acknowledgements

The author wishes to thank Prof. L. W. Morland from the University of East Anglia (UEA) in Norwich for helpful discussions during preparation of this work.

References

1. BIOT M.A., 1956,Theory of Propagation of Elastic Waves in a Fluid-Saturated Porous Solid. I Low Frequency Range. II Higher Frequency Range, *The J. of the Acoustical Soc. of America*, **28**, 2, 168-191
2. CHARLIE W., MARTIN J.P., SHINN J., BLOUIN S., MELZER S., 1980, Blast Induced Soil Liquefaction. Phenomena and Evaluation, *Proc. Int. Symp. on Soils under Cyclic and Transient Loading*, Swansea, A.A. Balkema, 533-542
3. COLE R.H., 1965, *Underwater Explosions*, Dover Publications Inc., New York
4. DAS B.H., 1983, *Fundamentals of Soil Dynamics*, Elsevier, New York-Amsterdam-Oxford
5. FINN W.D.L., 1982, Dynamic Response Analyses of Saturated Sands, *Proc. Int. Symp. "Soil Mechanics – Transient and Cyclic Loads"*, (edit. Pande and Zienkiewicz), Wiley, 105
6. FODA M.A., 1989, Sideband Damping of Water Waves over a Soft Bed, *J. Fluid Mech.*, **201**, 189-201
7. FRAGASZY R.J., VOSS M.E., 1982, Laboratory Modelling of Blast-Induced Liquefaction, *Proc. Soil. Dynamics and Earthquake Eng. Conf.*, Southampton, 873-886
8. GARG S.K., NAYFEH A.H., GOOD A.J., 1974, Compressional Waves in Fluid-Saturated Elastic Porous Media, *J. Applied Physics*, **45**, 5, 1968-1974
9. HUNT J.N., 1959, On the Damping of Gravity Waves Propagated over a Permeable Surface, *J. Geoph. Research*, **64**, 437
10. ISHIHARA K., TOWHATA I., 1982, Dynamic Response Analysis of Level Ground Based on the Effective Stress Method, *Proc. Int. Symp. "Soil Mechanics – Transient and Cyclic Loads"*, (edit. Pande and Zienkiewicz), Wiley, 133
11. LAMBE T.W., WHITMAN R.V., 1969, *Soil Mechanics*, Wiley, New York-London-Sidney-Toronto

12. LIU F.L., 1973, Damping of Water Waves over Porous Bed, *Proc. ASCE, J. Hydr. Div.*, **99** (HY 12), 2263-71

13. MADSEN O.S., 1978, Wave Induced Pore Pressures and Effective Stresses in a Porous Bed, *Geotechnique*, **28**, 4, 377-393

14. MALLARD W.W., DALRYMPLE R.A., 1977, Water Waves Propagating over a Deformable Bottom, *Offshore Tech. Conf. 2895*, Houston, Texas

15. MARTIN C.S., 1970, Effects of a Porous Sand Bed on Incipient Sediment Motion, *J. Water Resources Research*, **6**, 4, 1162-1174

16. MARTIN P.P., SEED H.B., 1982, One-Dimensional Dynamic Ground Response Analyses, *Proc. ASCE, J. Geot. Eng. Div.*, **GT7**, 935

17. MASSEL S.R., 1976, Gravity Waves Propagated over Permeable Bottom, *Proc. ASCE, J. Waterways, Harbors and Coastal Eng. Div.*, **102**, WW2, 11-21

18. MORLAND L.W., 1959, The Propagation of Plane Irrotational Waves through an Elastoplastic Medium, *Phil. Trans. Royal Soc. London*, Series A, No. 997, **251**, 341-383

19. MORLAND L.W., 1978, A Theory of Slow Fluid Flow through a Porous Thermoelastic Matrix, *Geophys. J. R. Astr. Soc.*, **55**, 393

20. MORLAND L.W., SAWICKI A., 1983, A Mixture Model for the Compaction of Saturated Sand, *Mechanics of Materials*, **2**, 203-216

21. MORLAND L.W., SAWICKI A., 1985, A Model for Compaction and Shear Hysteresis in Saturated Granular Materials, *J. Mech. Phys. Solids*, **33**, 1, 1-24

22. MOSHAGEN H., TØRUM A., 1975, Wave Induced Pressures in Permeable Seabeds, *Proc. ASCE, J. Waterways, Harbors and Coastal Eng. Div.*, **101**, WW1, 49-57

23. NOWACKI W.K., RANIECKI B., 1987, Theoretical Analysis of Dynamic Compacting of Soil Around a Spherical Source of Explosion, *Arch. Mech.*, **39**, 4, 359-584

24. PATERSON N.R., 1956, Seismic Wave Propagation in Porous Granular Media, *Geophysics*, **XXI**, 3, 691-714

25. PREVOST J.H., EIDE 0., ANDERSON K.H., 1975, Wave Induced Pressures in Permeable Seabeds, *Proc. ASCE, J. Waterways, Harbors and Coastal Eng. Div.*, **101**, WW4, 464-465

26. PUTNAM J.A., 1949, Loss of Wave Energy Due to Percolation in a Permeable Sea Bottom, *Trans. Am. Geophys. Union*, **30**, 349-356

27. RAWLINGS C.G., 1987, *Blast Induced Liquefaction of Soils. A Reference Search*, Norwegian Geotechnical Institute, 52209-1, Oslo

28. REID R.0., KAJIURA K., 1957, On the Damping of Gravity Waves over a Permeable Seabed, *Trans. Am. Geophys. Union*, **38**, 662-666

29. RICKER N.H., 1977, Transient Waves in Visco-Elastic Media, *Developments in Solid Earth Geophysics*, **10**, Elsevier, Amsterdam-Oxford-New York

30. SAWICKI A., MORLAND L.W., 1985, Pore Pressure Generation in a Saturated Sand Layer Subjected to a Cyclic Horizontal Acceleration at its Base, *J. Mech. Phys. Solids*, **33**, 6, 545-559

31. STUDER J., KOK L., 1980, Blast-Induced Excess Porewater Pressure and Liquefaction. Experience and Application, *Proc. Int. Symp. on Soils under Cyclic and Transient Loading*, Swansea, A.A. Balkema, 581-593

32. SYVITSKI J., SCHAFER C., 1990, *ADFEX – Environmental Impact Statement*, Geological Survey of Canada, Dartmouth.

33. VALLIAPAN S., ANG K.K., 1988, Numerical Modelling of Tunnel Blasting, in: *Numerical Methods in Geomechanics*, (edit. Swoboda, Innsbruck), A.A. Balkema, Rotterdam, 145-154

34. YAMAMOTO T., KONING H.L., SELLMEIJER H., HIJUM E. VAN, 1978, On the Response of a Poro-Elastic Bed to Water Waves, *J. Fluid Mech.*, **87**, part 1, 193-206

35. ZIENKIEWICZ 0.C., CHANG C.T., HINTON E., 1978, Non-Linear Seismic Response and Liquefaction, *Int. J. Num. Anal. Meth. Geomech.*, **2**, 381-404

Jednowymiarowa fala upłynnienia w nawodnionych piaskach

Streszczenie

Przedstawiono zastosowanie teorii zagęszczania do opisu propagacji jednowymiarowej fali upłynnienia w nawodnionych piaskach. Wykazano, że upłynnienie jest możliwe zarówno podczas procesu obciążenia jak i odciążenia w zależności od wielkości naprężeń oraz od właściwości mechanicznych materiału. Pokazano, że fala globalnego naprężenia propaguje się bez zmiany kształtu. Procesowi twmu towarzyszy przegrupowanie naprężeń parcjalnych w składnikach mieszaniny, tj. generowane jest ciśnienie porowe, któremu towarzyszy redukcja naprężeń efektywnych w szkielecie gruntowym. Zjawisko to prowadzi do upłynnienia nawodnionego gruntu.

Manuscript received April 29, 1997; accepted for print October 20, 1997